ELSEVIER

Contents lists available at ScienceDirect

NDT and E International

journal homepage: www.elsevier.com/locate/ndteint





Microwave imaging sensor system using metamaterial lens for subwavelength resolution

Srijan Datta*, Lalita Upda

Nondestructive Evaluation Laboratory, Michigan State University, East Lansing, MI, 48824, USA

ARTICLE INFO

Keywords:
Coherent detection
Lenses
Metamaterials
Microwave imaging
Nondestructive testing

ABSTRACT

Lenses made of negative refractive index metamaterials can overcome the diffraction-limited resolution of imaging at working distances in the far-field. This paper describes a novel negative index metamaterial (NIM) lens imaging sensor system for subwavelength microwave nondestructive evaluation (NDE) using homodyne detection measurements. The split-ring resonator (SRR) - wire based NIM lens is optimized to work at 6.3 GHz (wavelength $\lambda=48$ mm). Coherent homodyne detection scheme provides a simple, low-cost, and highly sensitive NIM lens imaging sensor system that can be used in the field under practical conditions. Imaging of an omnidirectional source using negative refraction is shown using the proposed system. A focal spot of size 0.62 λ was obtained in the image plane of the metamaterial lens with a source to image distance of 1.67 λ . The focal spot position was further shifted in the azimuthal plane by simple movement of the source. The study demonstrates unique focus-scanning capability of NIM lenses for target localization without the need for complex tuning mechanisms. The feasibility of the system to image subwavelength defects inside dielectric materials in reflection mode is also investigated for its potential application as an NDE sensor. Defects comprising subwavelength hole of diameter 0.25 λ and a groove of dimensions 0.31 λ x 0.1 λ placed at the focal plane of the lens was imaged using the proposed sensor system.

1. Introduction

Microwaves are widely used in a variety of imaging and sensing applications due to their ability to penetrate non-conducting or dielectric materials. Biomedical imaging for cancer cell detection, characterization of dielectric fluids, security screening for concealed weapons detection, ground penetrating radar and remote sensing for geological objects, structural health monitoring and nondestructive testing [1-7] are some of the applications of microwaves. Microwave imaging can be implemented in far-field and near-field modes depending on the distance between the source and test object. In far-field mode, the imaging resolution is limited by the physics of diffraction [8]. Objects smaller than the operating wavelength λ are generally not detected in far-field since a conventional lens cannot focus waves onto an area smaller than $\lambda 2$. In contrast, near-field microwave imaging sensors can provide subwavelength resolution. However, the probe working distance is limited to proximity of the object (in order of $\lambda/10$) for near-field imaging [9]. Use of lenses made of negative refractive index metamaterials can bridge the gap between the two imaging modes by providing subwavelength resolution beyond the diffraction limit at far field working distances [10].

Idea of negative refractive index materials was discussed as early as beginning of the 20th century when Schuster showed that negative refraction takes place at the boundary of two media, one supporting a forward wave and the other one a backward wave [11]. Present-day research in metamaterials was stimulated by the theoretical work of Veselago et al. in the 1950s [12-14] and later by the realization of engineered metamaterials by Smith et al. at the turn of the century [15–18]. Since then, metamaterials have been extensively researched as means of controlling the propagation of EM waves ranging from microwave to optical frequencies [19]. They are engineered materials which consist of a periodic arrangement of subwavelength scatterers or unit cells. An incident EM wave will be myopic to the inhomogeneity of such periodic materials if the periodicity is much smaller than the wavelength. Based on effective medium theory, the unit cell size a should be less than $\lambda/4$ for such inhomogeneous periodic materials to behave like a homogenous medium with an effective permittivity and permeability [20,21]. The unit cells of metamaterials have also been

E-mail address: dattasri@msu.edu (S. Datta).

^{*} Corresponding author.

referred to as meta-atoms in view of their analogy to atoms of conventional materials. The effective EM properties of metamaterials depends on the design and arrangement of unit cells in contrast to material composition in atomic scale like that of dielectric materials. Hence, they can be tailored to have specialized EM characteristics including negative refractive index that is useful in novel lensing applications. Pendry showed theoretically in Ref. [22] that a slab made of negative index metamaterials (NIM) can act as a "perfect lens" for a diverging source as both the propagating and evanescent wave components of the EM field will contribute to the resolution of the image. Although losses associated with engineered metamaterials makes it impossible to realize perfect lensing conditions [23,24], sub-diffraction imaging using NIM lenses is still achievable as shown by various studies [25–28].

This paper describes the design of a novel NIM lens imaging sensor system for microwave NDE of subwavelength defects. Existing literature on using metamaterials for microwave NDE has mostly involved metamaterial inspired structures for near field sensing applications [29–36]. One prior study on using NIM lenses for far-field microwave NDE was done by Shreiber et al., where they presented the detection of subwavelength defects at a working distance of 1.9λ [37]. However, the NDE measurements was performed using a Vector Network Analyzer (VNA) in a semi-anechoic environment, which may not be practical for industrial implementation. The NIM lens was embedded in microwave absorbers to isolate the transmitter and receiver. Moreover, high frequency amplifiers were required since the directivity of diverging sources is weak and engineered NIM lenses are highly dispersive structures. This paper presents a system using homodyne measurement techniques with NIM lenses to provide a NDE imaging system that can be used in the field. Using the proposed system, subwavelength defect imaging of dielectric materials in transmission mode has already been reported [38,39].

This contribution focuses on imaging of subwavelength defects in reflection mode to demonstrate the feasibility of the system for imaging in single side access. Reflection mode microwave NDE results of subwavelength defects using NIM lenses are reported for the first time in literature. Reflection mode imaging provides a practical system that can be deployed in the field as in most instances, there is single side access to the samples under test. Further, 2D NDE scans are reported in this paper to demonstrate the ability of the proposed system for imaging defects in addition to detection capabilities reported in Ref. [38]. The lens design is similar to Ref. [38] but scaled to work at a higher frequency band. The resolution of the lenses is dependent on the operating wavelength. Therefore, a shorter wavelength design is considered in this study to demonstrate the scalability of the NIM lens designs for detection of smaller defects in composite samples. Fig. 1 presents the schematic of the proposed microwave NDE sensor for imaging of subwavelength defects. A transmitting monopole antenna is placed in the front focal plane of the NIM lens. The diverging waves from the antenna are bought to focus by the lens at its second focal plane where the dielectric material

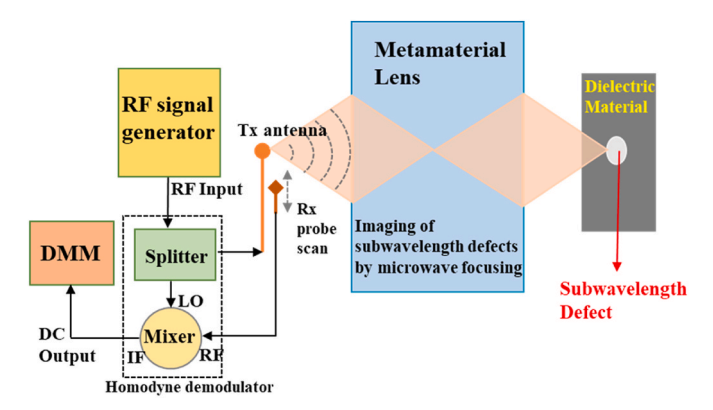


Fig. 1. Proposed microwave imaging sensor system.

under test is positioned. The reflected rays from the dielectric material can be sampled at the front focal plane in reflection mode to collect high spatial frequency information and image subwavelength defects. Coherent homodyne detection provides stable access to the information encoded in the phase data by supressing the excessive noise components [40,41]. High signal to noise ratio associated with such synchronous detection allows the implementation of dispersive NIM lenses in free space under practical conditions without the use of amplifiers or microwave absorbers. Demodulating the image signal into a measurable dc signal also reduces the complexity of the imaging system and hence provides a rapid, low cost solution [42].

The paper is organized as follows. Section 2 briefly discusses the working principles of NIM lenses and how they can be used to overcome the resolution limit of conventional lenses. Section 3 presents the unit cell simulation study and experimental validation of the metamaterial lens design. In section 4, microwave imaging results obtained using the proposed system is reported. Source imaging as well as subwavelength defect imaging results are presented in this section.

2. Principles of metamaterial lens imaging

An object is visible because it either emits or scatters EM radiation. The problem of imaging an object is concerned with reproducing the EM field distribution of the object in an image plane. Consider a 2D monochromatic object in the x-y plane placed at z=0. The field distribution $\psi(x,y,z)$ of the object in free space can expressed as a superposition of all possible elementary plane waves given by the 2D Fourier spectrum

$$\psi(x,y,z) = \iint_{-\infty}^{+\infty} \psi_F(k_x,k_y) e^{i(k_x x + k_y y + k_z z)} dk_x dk_y$$
(1)

where $\psi_F(k_x,k_y)$ are the spatial frequency components of the object. Maxwell's equations tell us that $k_z = \sqrt{\frac{\omega^2}{c^2} - k_x^2 - k_y^2}$, where ω is the frequency of the source and c is the speed of light. For spatial frequencies $k_x^2 + k_y^2 < \frac{\omega^2}{c^2}$, k_z is real, leading to propagating waves of the field in the z direction. As we move out of the object plane along the z direction, the field distribution will change. As a consequence, the Fourier spectrum on the observation (image) plane will no longer resemble the object Fourier spectrum. The function of a lens is to apply phase correction to the radiative Fourier components of the object so that the fields reassemble to a focus, and an image of the object appears at the focal plane of the lens. However, for larger values of transverse wave numbers, corresponding to high spatial frequency, i.e. $(k_x^2 + k_y^2 > \frac{\omega^2}{c^2})$, k_z is imaginary leading to non-propagating evanescent waves. These evanescent waves, containing the higher spatial frequency information, attenuate exponentially with distance from the object. Conventional lenses can focus only the propagating waves and the evanescent wave spectrum of the object field is essentially removed from images in the far-field. Since propagating waves are limited to $k_{\rm x}^2 + k_{\rm y}^2 < \frac{\omega^2}{c^2}$, the maximum resolution Δ_F achievable by a conventional lens image is

$$\Delta_F \approx \frac{2\pi}{k_{max}} = \frac{2\pi c}{\omega} = \lambda \tag{2}$$

and the diffraction limit manifests itself as an image smeared over an area of approximately one wavelength in diameter. It was shown in Ref. [20] that a slab made of negative refractive index material can act as a "perfect lens" as it can amplify the evanescent wave components along with bringing into focus the propagating waves. Fig. 2 describe the working principles of a negative refraction lens. Negative refraction through the flat lens will bend the diverging rays from an object towards optical axis. The rays will converge once inside the lens, and then at a focal spot outside the lens where an image of the object will be formed

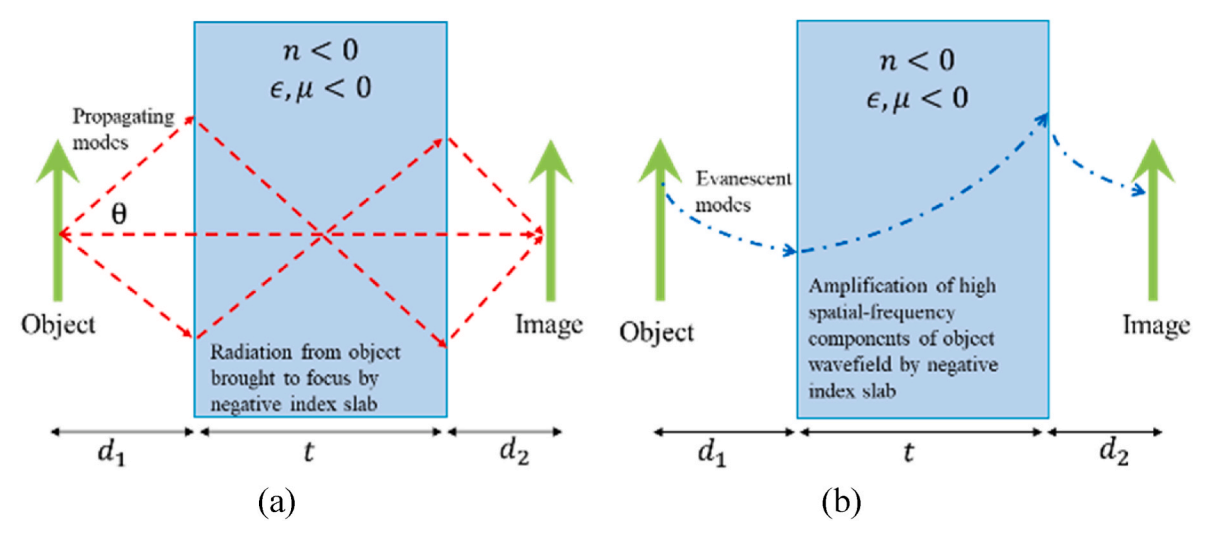


Fig. 2. NIM lens working principle (a) Focusing of propagating waves (b) Amplification of evanescent wave components.

(Fig. 2a). In addition to bringing into focus the propagating rays, the evanescent wave components will also be amplified by the negative index slab, and the high spatial frequency information can be recovered in the image plane (Fig. 2b). Hence, a perfect image of the object can be obtained at the focal plane of such a lens as all the Fourier components will contribute to the resolution of the image. Using geometric optics, it can be shown that an object placed at a distance d_1 (front focal length) from a slab of thickness t with an arbitrary negative refractive index t0 will be bought to focus at a distance t2 (second focal length) given by Ref. [43],

$$d_2 = \frac{n_s \cos(\theta)t}{\sqrt{n^2 - n_s^2 \sin(\theta)}} - d_1 \tag{3}$$

where n_s is the refractive index of the surrounding medium and θ is the angle of incidence (Fig. 2a).

The conditions under which perfect imaging will occur is given by

$$\varepsilon = -\varepsilon_s, \mu = -\mu_s \tag{4}$$

where ε and μ are the dielectric permittivity and magnetic permeability respectively of the negative index slab, and ε_s and μ_s are the corresponding quantities of the surrounding medium. The refractive index, n of any material is given by

$$n = \pm \sqrt{\mu \varepsilon} \tag{5}$$

The negative square root in the calculation of n is chosen in equation (5) when both ε and μ are negative to account for propagation of backward waves in negative index medium [44]. Therefore, the refractive index n of a perfect lens in free space equals -1 and equation (3) reduces to $d_2 = t - d_1$.

Although in theory a perfect image reconstruction of an object can be

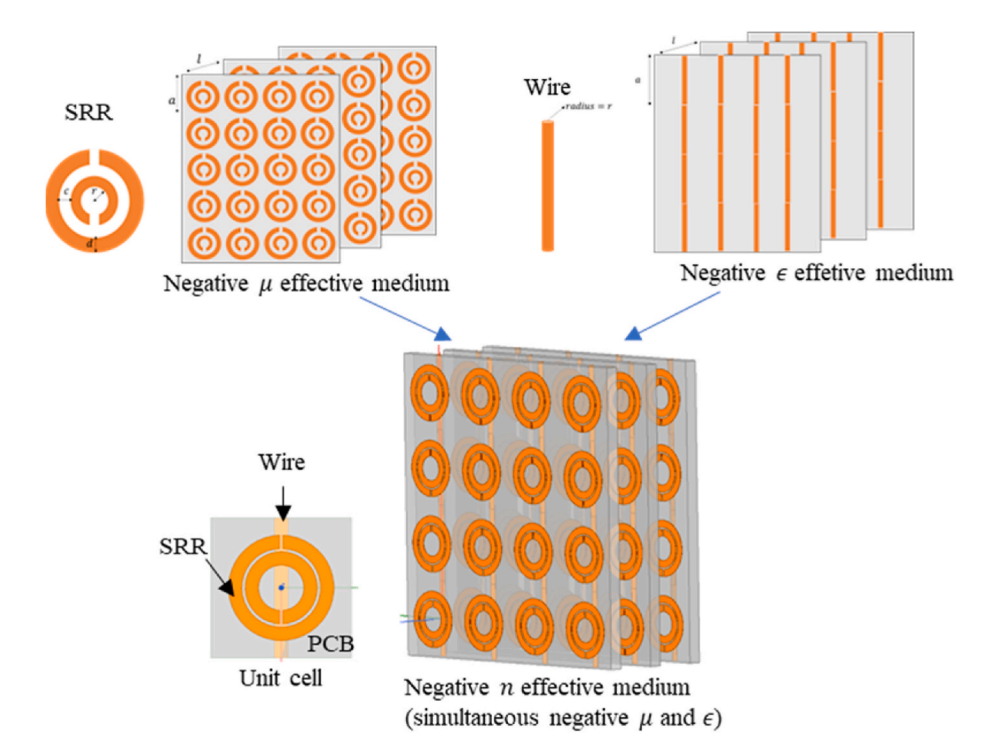


Fig. 3. NIM Lens effective medium implementation on PCB technology. The periodic arrangement of SRR-wire unit cells will exhibit negative refractive index frequencies to specific incident wave polarization over a prescribed range of frequencies.

obtained in this way using a lossless n=-1 slab, it is impossible to achieve these idealized conditions in practice. Losses associated with engineered metamaterials degrades the perfect resolving capabilities of NIM lenses. However, overcoming the diffraction barrier is still achievable using engineered NIM lenses [45]. The EM metamaterial concept was extended to acoustic engineering as well [46], with several studies demonstrating subwavelength imaging using acoustic metamaterial lenses [47,48].

3. Metamaterial lens design

A NIM can be implemented in the microwave frequencies as an effective medium using a periodic array of SRR and wire unit cells (Fig. 3). A periodic array of the SRRs will behave like a magnetic plasma in the microwave frequencies under the excitation by an external magnetic field parallel to the axis of the SRRs [16]. The effective permeability of an SRR array is given by

$$\mu_{eff}(\omega) = 1 - \frac{\omega_{mp}^2}{\omega^2} \tag{6}$$

where ω_{mp} is the magnetic plasma frequency and ω is frequency of the excitation field. Equation (6) shows that μ_{eff} is negative for frequencies $\omega < \omega_{mp}$ and propagating wave modes are prohibited in this frequency band due to the negative μ_{eff} of the SRR medium.

A periodic array of the thin metallic wire elements under the influence of a time-varying electric field, can mimic an electric plasma at microwave frequencies [17]. The effective relative permittivity of such an array in the presence of an external electric field parallel to the wires is given by

$$\varepsilon_{eff}(\omega) = 1 - \frac{\omega_{ep}^2}{\omega^2} \tag{7}$$

where ω_{ep} is the electric plasma frequency of the wire medium, and ω is frequency of the excitation field. Equation (7) shows that the real part of ε_{eff} has negative values for frequencies $\omega < \omega_{ep}$. This causes the wire medium to prohibit propagating modes in that frequency range.

Combining both the SRR and wire elements in a periodic array gives rise to a metamaterial medium having simultaneous negative μ_{eff} and ε_{eff} over a certain range of frequencies [15]. A left-handed $(\overrightarrow{E}, \overrightarrow{H})$ and \overrightarrow{k} form a left-handed triplet) transmission band occurs within the previously overlapping forbidden bands of negative μ_{eff} and negative ε_{eff} . The combined array behaves as a medium having an effective negative refractive index in this transmission band, and the transmission peak is referred to as a left-handed peak.

3.1. Unit cell simulation

Since the EM characteristics of a metamaterial is determined by its unit cell, a NIM can be designed by simulating an infinite array of the

unit cells using periodic boundary conditions [49]. Commercial finite element method (FEM) solver Ansys HFSS was used to design and optimize the SRR-wire unit cell. The unit cell model of the NIM lens design along with the incident wave polarization is shown in Fig. 4a. The \overrightarrow{H} field is polarized into the plane of the SRRs (z direction) while the \overrightarrow{E} field is polarized parallel to the wires (x direction) to generate the required EM response for negative refractive index. The Perfect E and Perfect H boundary conditions of HFSS were applied on the y-z and x-y boundaries of the unit cell model, respectively, to mimic an infinite array of unit cells and ensure correct polarization of the incident wave. Wave ports were assigned on the z-x boundaries to excite the model with a plane wave and obtain the S-parameters of the metamaterial design. The unit cell is optimized to operate around 6.3 GHz on a 0.6 mm thick FR4 ($\varepsilon_r = 4.4$) PCB substrate. The dimensional parameters for the unit cell model are: a = 4 mm, r = 0.9 mm, t = 0.4 mm, w = 0.4 mm, g = 0.2mm, c = 0.2 mm (Fig. 3b). The distance between consecutive PCB layers is set to be 3.4 mm. The simulated scattering parameters for the unit cell design using Ansys HFSS is shown in Fig. 5a. A transmission band is obtained around 6.3 GHz with a transmission peak of -1.08 dB. To verify the left-handed nature of the transmission band, EM parameter retrieval from the simulated S parameters is performed. The parameter retrieval method is based on the well-established Nicholson Ross Weir method and is described in the Appendix of [38]. The extracted EM parameters are also plotted in Fig. 5. The real part of the refractive index for the proposed NIM lens is -3.33 at the operating frequency of 6.3 GHz (Fig. 5b). The real part of μ and ε are simultaneously negative in this band (Fig. 5c and d), rendering the refractive index n to be negative (equation (5)).

3.2. Experimental validation

An NIM lens, consisting of $N_x=20$, $N_y=10$ and $N_z=30$ unit cells, was fabricated for experimental validation of the lens design. Fig. 6 presents the fabricated metamaterial lens. Each PCB layer consists of 20×10 unit cells and 30 such layers were stacked at intervals of 3.4 mm using 3D printed holder with slots. The final dimensions of the lens are $80 \text{ mm} (1.67\lambda) \times 40 \text{ mm} (0.83\lambda) \times 100 \text{ mm} (2.08\lambda)$. The thickness t of the fabricated lens in direction of incident wave propagation is 40 mm.

Frequency sweep measurements were performed at the beginning using an Agilent EB070B VNA to experimentally determine the left-handed transmission peak of the fabricated lens. Two wideband, double ridged horn antennas (TDK HRN-0118) were used as the transmitter and receiver to ensure correct polarization of the incident EM waves. A large metallic screen with a window of the size of the lens was used to perform the measurements (Fig. 7a). The magnitude of S_{21} parameter calibrated with free space measurements are shown in Fig. 7b. A left-handed peak transmission of -1.5 dB is observed around 6.3 GHz. Conventional right-handed transmission band is obtained above 9.5 GHz. The refractive index of the lens is positive in that frequency region as shown in Fig. 5c.

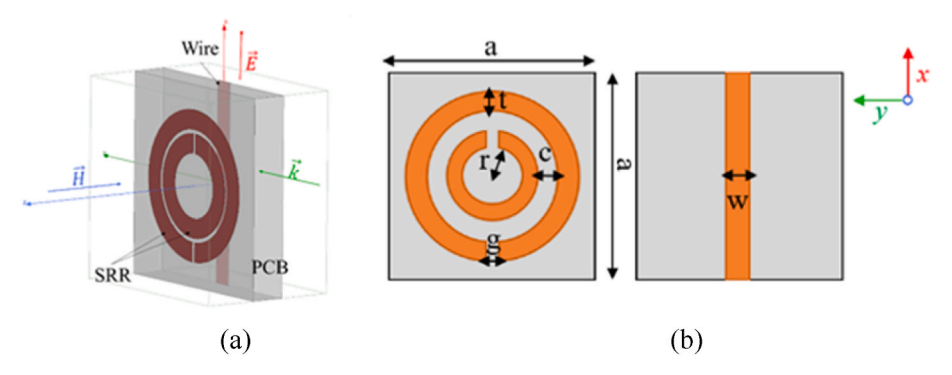


Fig. 4. NIM Lens unit cell (a) Ansys HFSS model (b) Schematic.

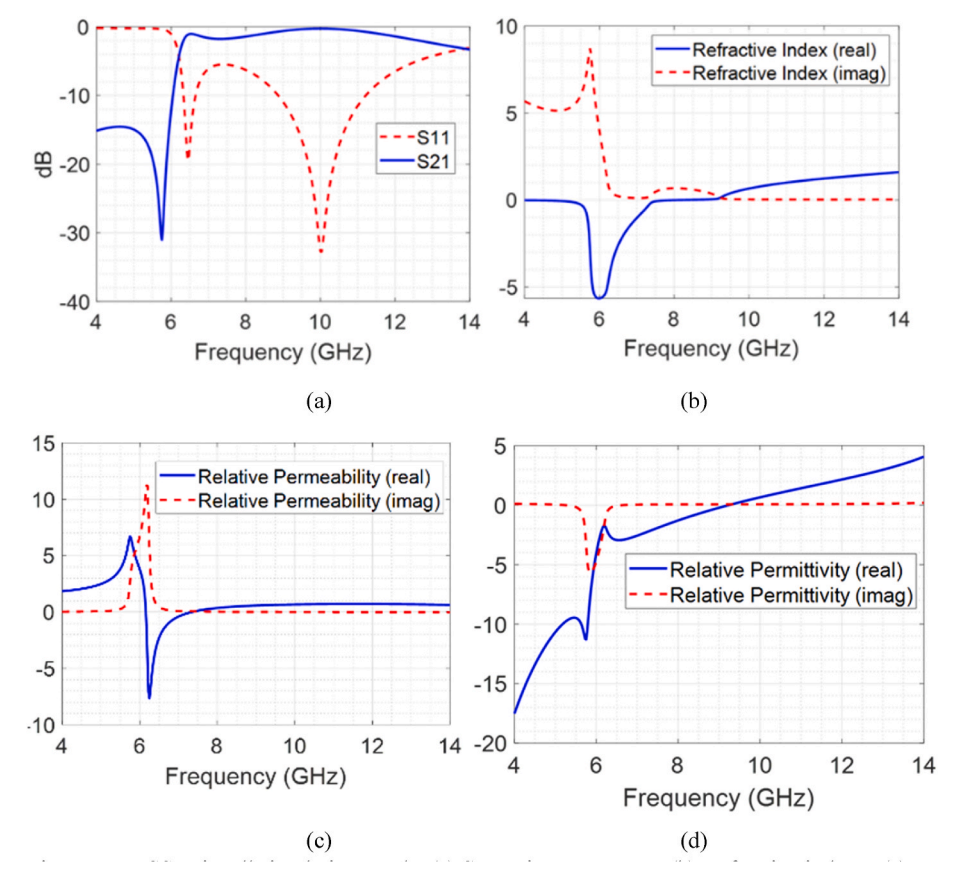


Fig. 5. HFSS unit cell simulation results (a) Scattering parameters (b) Refractive index n (c) Permeability μ (d) Permittivity ε .

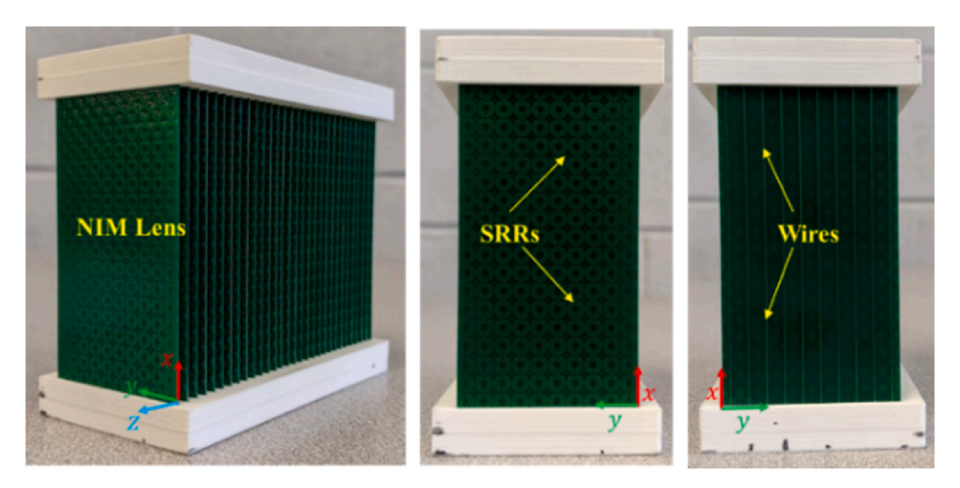


Fig. 6. Fabricated metamaterial lens.

4. Microwave imaging experiments

Once the left-handed peak frequency of the metamaterial lens was determined experimentally using a Network Analyzer, single frequency measurements using the homodyne detection system was done to perform imaging experiments. The RF signal generator was used to excite the experiment setup at left-handed peak frequency of 6.3 GHz with an output power of 10 dBm. The received signal intensity distribution was measured as a voltage reading in the order of 1 mV by the DMM. The voltage distribution in space will be proportional to the image field distribution and therefore can be visualized to obtain the desired image. Details of operation of coherent homodyne detection are presented in the appendix section. The units of the color bar in all the

reported imaging results correspond to the raw voltage (in Volts) recorded by the DMM.

4.1. Source imaging

Source imaging experiments using a transmitting monopole antenna was done to obtain the focal spot and verify negative refraction focusing by the flat NIM lens. The source imaging experiment setup and schematic is shown in Fig. 8. A monopole antenna produces an azimuthally symmetric field pattern, as does an ideal isotropic radiator. Diverging rays from the monopole antenna will be bought to focus by the NIM lens as described in Fig. 2. A quarter wavelength monopole was used as the receiving probe to sample the EM field. The receiving probe was

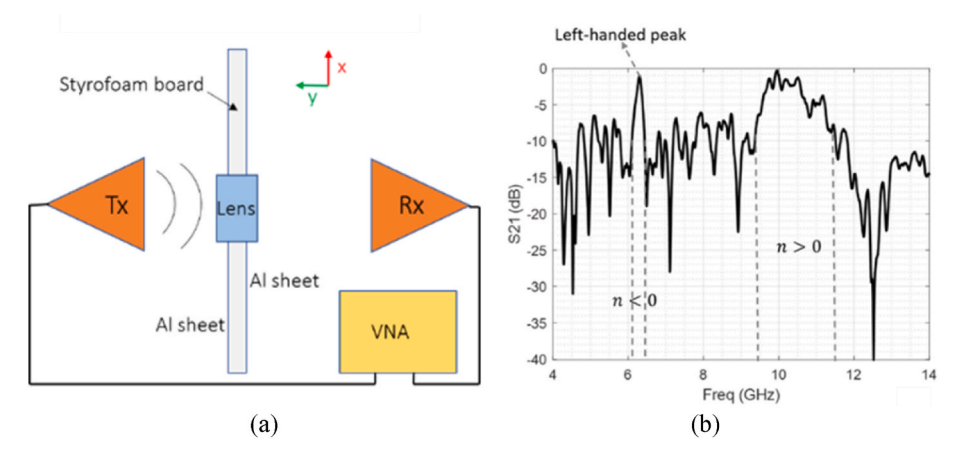


Fig. 7. (a) Transmission parameters experiment schematic (b) S21 calibrated with free space measurements.

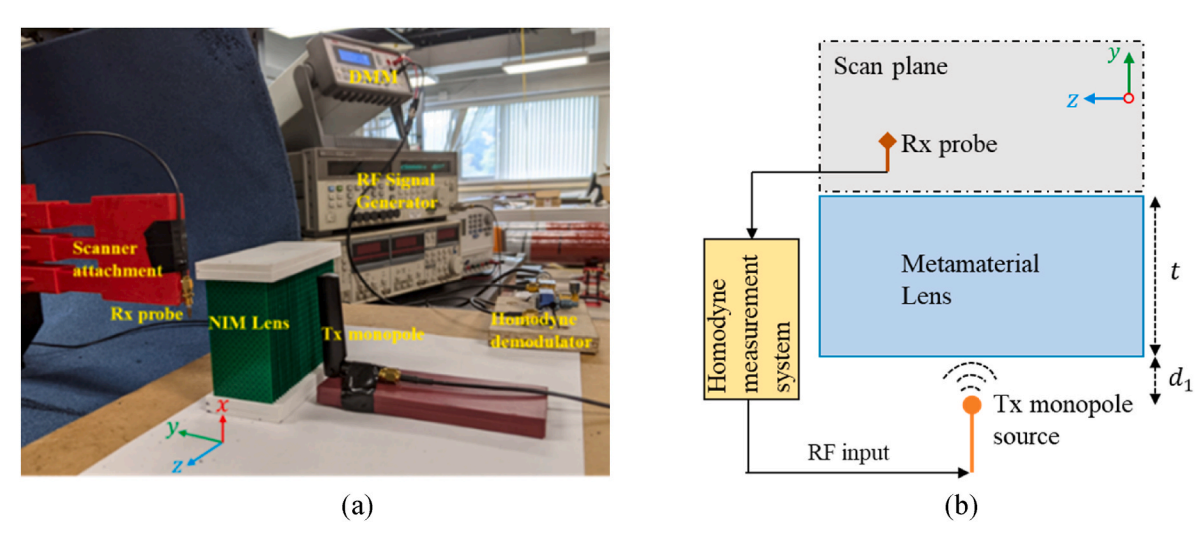


Fig. 8. Source imaging experiment (a) setup (b) schematic.

mounted on a computer controlled scanner to measure the field distribution after the waves pass through the lens. The scanning was done in the *y-z* plane with a step size of 5 mm in both directions.

Fig. 9a plots the imaging results with the source antenna placed 5 mm (d_1) away from the NIM lens. A focal spot is observed around 35 mm (d_2) which corresponds to the image of the monopole in the azimuthal plane. The experiment is performed in free space by removing the NIM lens to validate the negative refraction focusing by the lens. The free space image results (Fig. 9b) show the diverging radiation pattern of the source as expected. The cross-range intensity profiles for the two cases are plotted in Fig. 9c. The full width at half maxima (FWHM) for the focal spot is found to be 30 mm (0.62 λ). The FWHM at the focal plane without the lens is 67 mm (1.39 λ) indicating resolution enhancement by a factor of 2.24 ($\Delta_{lens}/\Delta_{free}$) is achieved with the lens.

The focal spot position of a NIM lens can be adjusted in the cross-range and down-range directions by moving the source object. This is an added novelty to the operation of NIM lenses, as focal spot scanning can be achieved without any complex tuning methods [50]. The source was first moved away from the NIM lens and kept at a distance of 15 mm (d_1) . The focal spot in this case is found to be at 20 mm (d_2) , clearly indicating a shift in the down-range direction (Fig. 10a). The focal spot moves closer to the lens as the source is moved away from the lens, which is consistent with the imaging theory discussed in Section 2 (equation (3)). Also, laterally shifting the source shifts the focal spot laterally. This was demonstrated by moving the source right of the optical axis (along z direction) by 10 mm. The imaging results for this case

show a cross-range shift of the focal spot by approximately the same distance (Fig. 10b). These results signify that the NIM lens system can be used for source (or defect) localization techniques as well when the position of the source is unknown. It is important to note that the focusing performance degrades as the source is moved away from the optical axis, as seen in the comparison in Fig. 10a and b. This is due to the increase of diffraction effects from the edges of the lens as the source is moved towards the sides. Therefore, the range of movement of the focal spot is restricted by the thickness of the lens in the down range direction (equation (3)) and by the aperture of the lens in the cross range direction (edge effects).

4.2. Subwavelength defect imaging

The capability of proposed system for microwave NDE of subwavelength defects beyond diffraction limit is demonstrated in this section. The schematic of experimental setup for microwave NDE in reflection mode is shown in Fig. 11. The reflected waves from the material under test placed at second focal plane (d_2 distance from lens) can be imaged at the first focal plane (d_1 distance from lens), where the transmitter and receiver are placed. Subwavelength defects inside the dielectric sample can be imaged by performing background subtraction of signals from a healthy sample. The measured voltage difference at the focal plane will correspond to the contributions due to the defect and can be plotted in a 2D graph to obtain the image of the defect. Two sets of NDE experiments are performed on two types of subwavelength

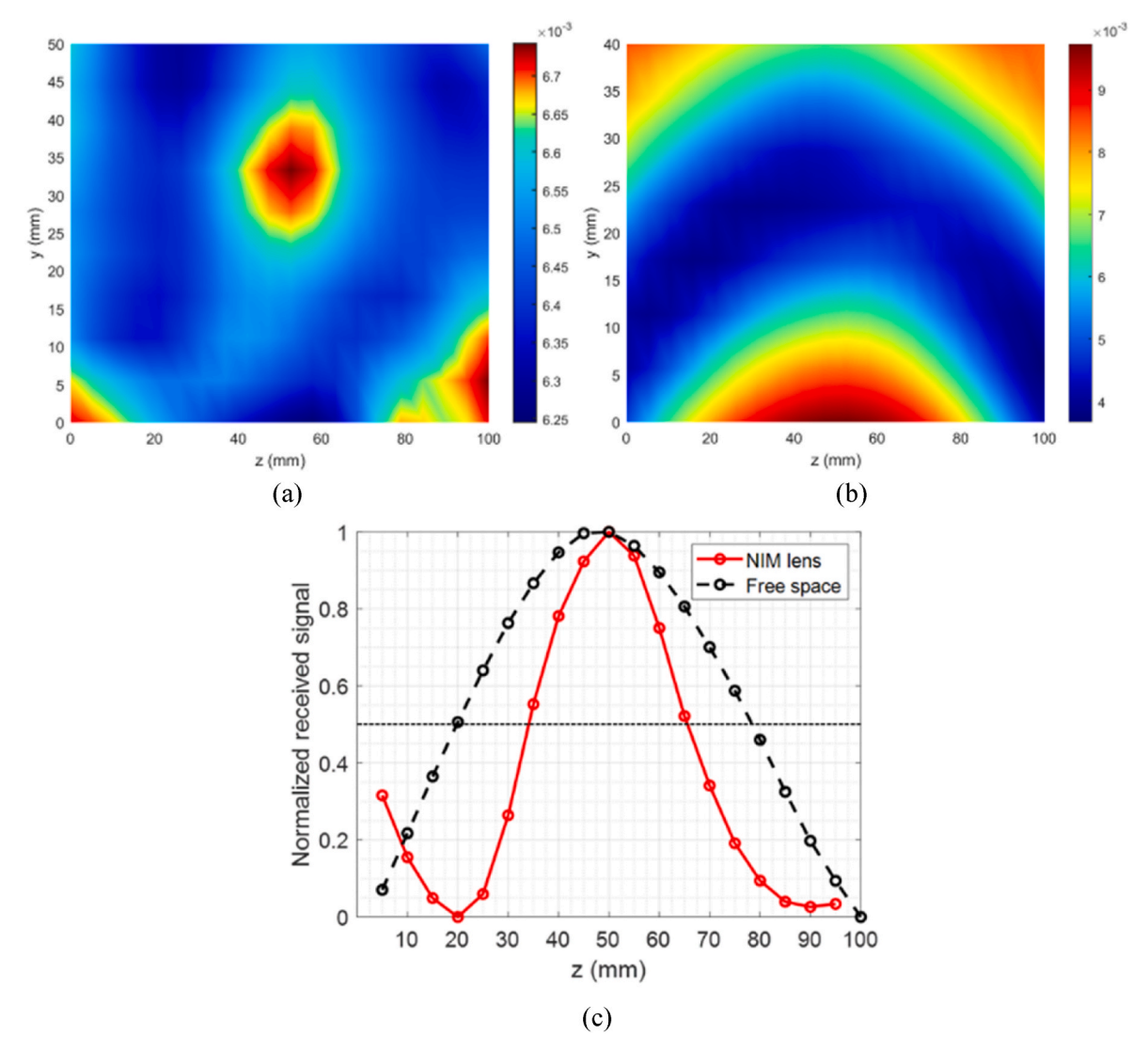


Fig. 9. (a) Source imaging with NIM lens (b) Source imaging without NIM lens (c) Comparison of cross-range intensity profiles of the images with and without lens.

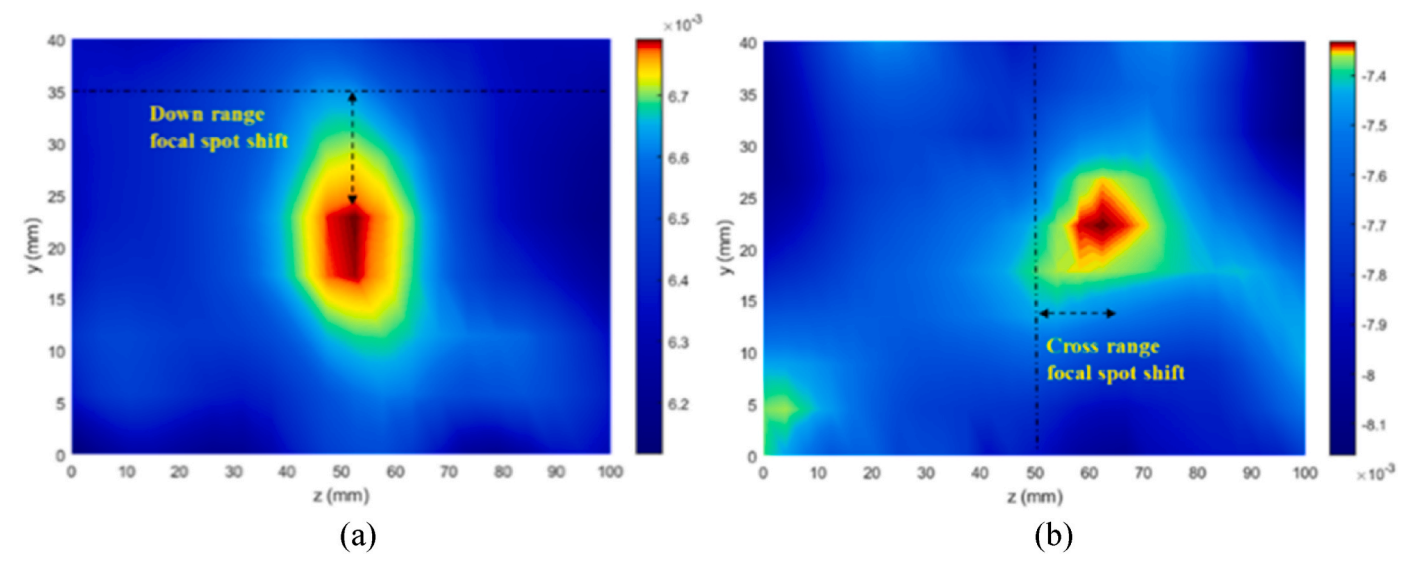


Fig. 10. Focal spot shift in (a) Down range direction (b) Cross range direction.

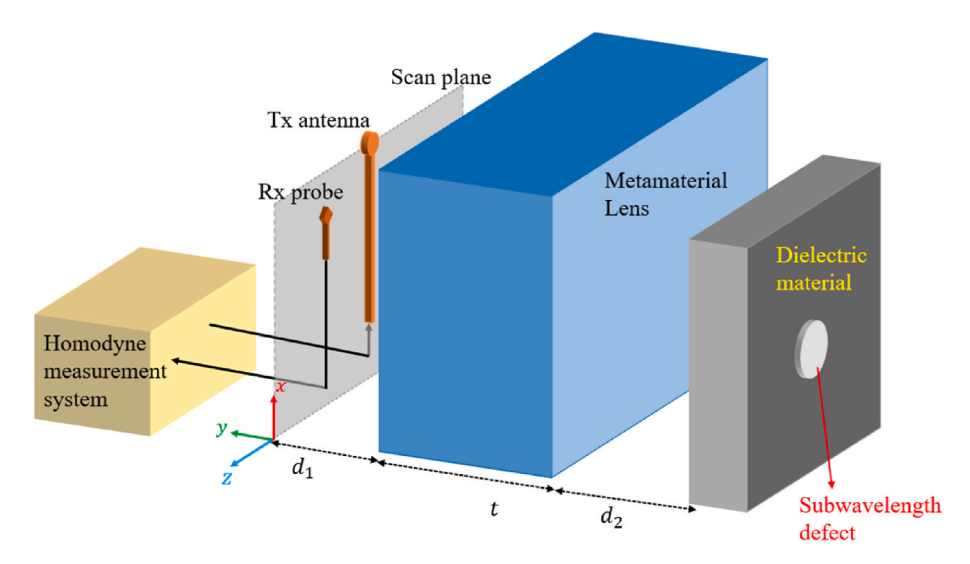
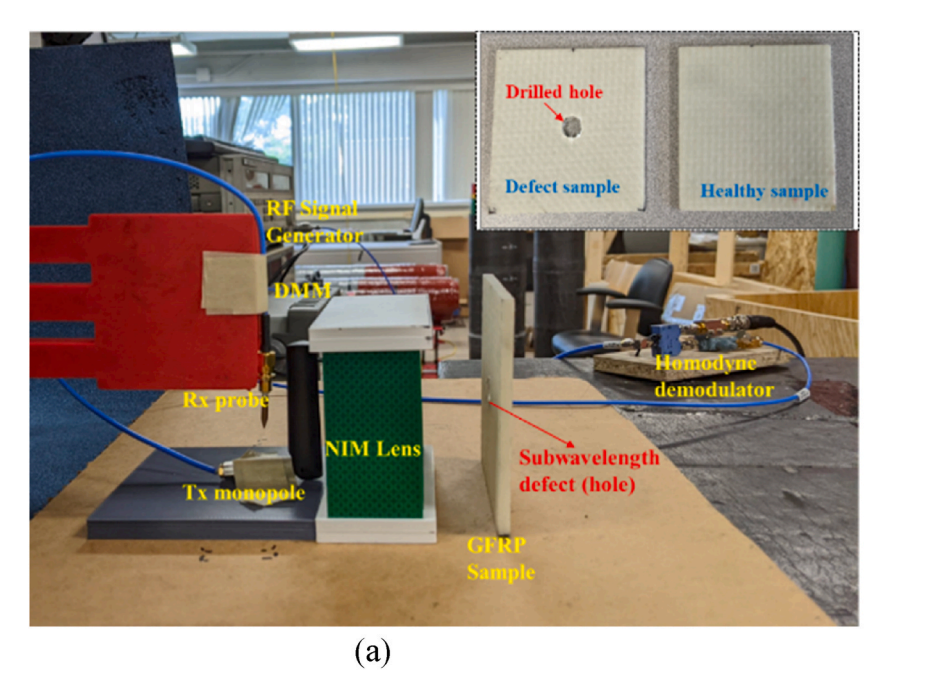


Fig. 11. Schematic of Microwave NDE experimental setup.

defects: holes and grooves.

A drilled hole of diameter 12 mm (0.25 λ) in a glass fiber reinforced polymer (GFRP) composite sample is tested first. The GFRP sample is of dimensions 100 mm \times 100 mm with a thickness of 8 mm. The experiment setup is shown in Fig. 12a and the sample schematic is shown in Fig. 12b. A similar sample without any drilled hole is treated as the healthy sample for obtaining the baseline signal for subtraction (inset of Fig. 12a). The receiver is scanned in the first focal plane (x-z at d_1) near the source with a step size of 2 mm in both directions. The imaging result for the drilled hole is reported in Fig. 13a. The presence of subwavelength defect is clearly imaged as indicated by the maxima (location y = 35 mm, z = 50 mm) of the image. The probe to defect standoff distance is 80 mm (1.67 λ), which is in the far-field. The experiment was performed without the NIM lens to demonstrate that the subwavelength defect is not detectable in the far-field at large stand-off distances. The imaging result in free space is shown in Fig. 13b. No detectable variation in measurements is observed in this case and the subwavelength defect goes undetected.

Next, imaging study of a groove of subwavelength dimensions was performed. The sample under test is composed of a Teflon block of dimensions 150 mm \times 150 mm and a thickness of 30 mm, mounted on an aluminum sheet to simulate a metal-composite joint [51]. Metal-composite joints are prone to disbond defects since air gaps can be introduced in the bonding epoxy layer during manufacturing or usage. Microwaves offer an attractive solution to NDE of such disbonds in metal composite joints and has been undertaken by various studies [52-54]. The purpose of this study is to show that subwavelength grooves, which are not typically detectable in the far-field, can be imaged using the proposed system. The simulated disbond is created by machining a groove of dimensions 15 mm (0.31λ) x 5 mm (0.1λ) along the entire length of the sample. The experiment setup and sample schematic are presented in Fig. 14. Similar to the earlier experiment, the sample with defect is placed at the second focal plane of the lens and the receiver is scanned in the first focal plane with a step size of 2 mm. A Teflon sample without any groove is treated as the healthy sample. Similar to the earlier experiment, the sample with defect is placed at the second focal



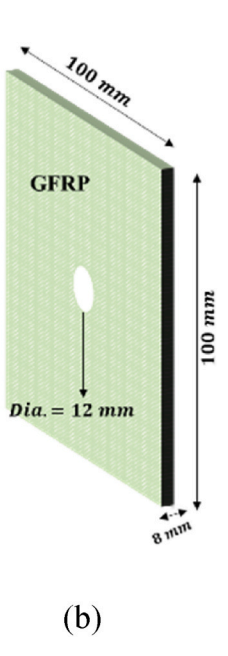


Fig. 12. (a) Experiment setup for subwavelength hole imaging (b) GFRP composite sample under test.

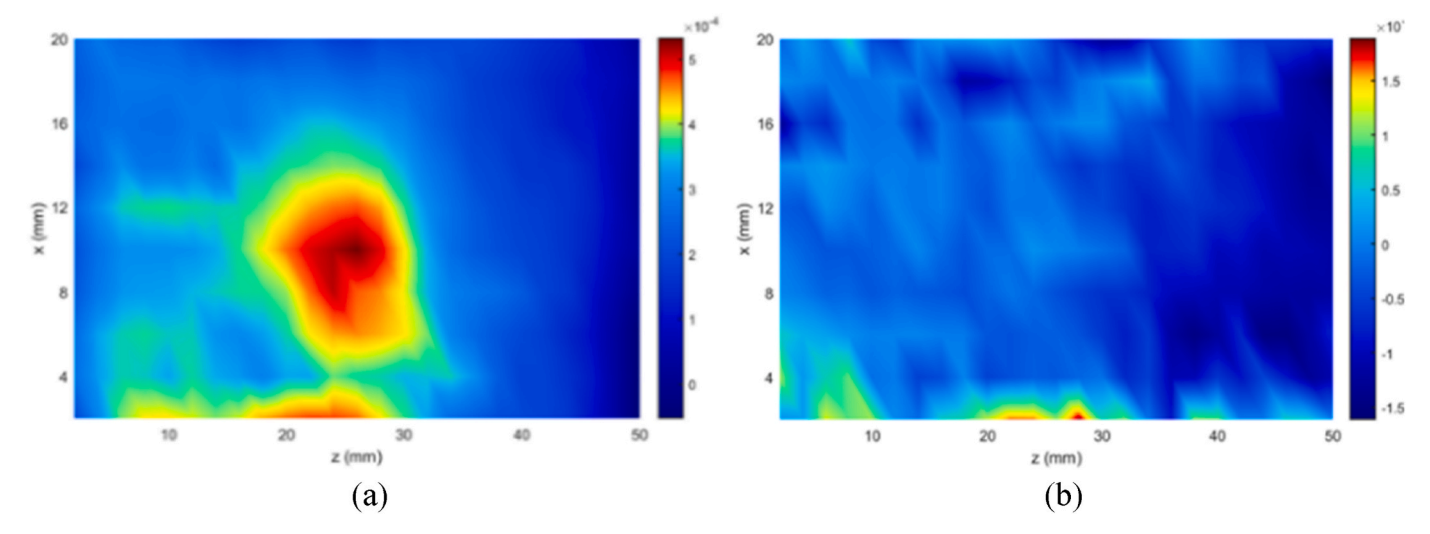


Fig. 13. Imaging results (a) with lens (b) without lens.

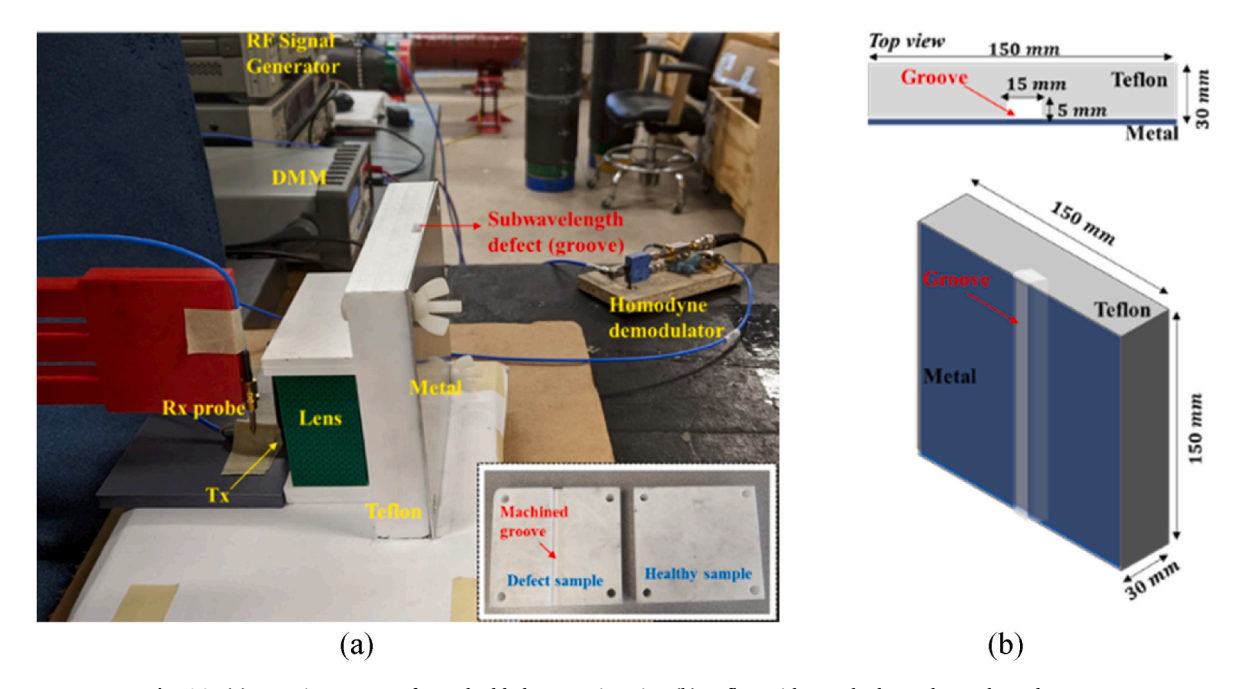


Fig. 14. (a) Experiment setup for embedded groove imaging (b) Teflon with attached metal sample under test.

plane of the lens and the receiver is scanned in the first focal plane with a step size of 2 mm. A Teflon sample without any groove is treated as the healthy sample (inset of Fig. 14a) for baseline subtraction. The defect image results with the lens are plotted in Fig. 15a. A stretched out maxima is observed at the center, indicating the presence of the groove. The NDE experiment is repeated without the lens and the corresponding results are shown in Fig. 15b. Absence of any discernible maxima in free space measurements further validate that subwavelength defects in dielectric materials, which are undetectable in far-field, can be imaged using a properly designed NIM lens.

5. Conclusions

Metamaterials exhibiting negative refractive index can act as "superlenses", which can achieve resolution capabilities beyond diffraction limits. Such a lens not only focuses the propagating wave modes emitting (scattering) from a source (object), but also amplifies the evanescent wave modes, which contain sub-diffraction information of

the object. The recovery of evanescent wave modes in the image plane of NIM lenses allows subwavelength source resolution at distances beyond the near-field of the object.

This paper presents a novel experimental implementation of such NIM lenses using coherent homodyne detection measurements for Microwave NDE applications. High SNR associated with synchronous detection provides a NIM lens imaging sensor system that can be used in the field at far-field distances under practical conditions. The metamaterial lens design is described followed by its implementation as subwavelength defect imaging sensor. Source imaging as well as subwavelength defect imaging results beyond the diffraction limit is experimentally reported using the proposed sensor system. Discussion on unique focal spot scanning capability of NIM lenses is also presented to demonstrate their added novel advantage over other lens designs.

Future work will include further experimental testing of defect detection range of the system. The resolution of NIM lenses is limited by the losses associated with such engineered structures. Lossy FR4 PCB was used to demonstrate proof of concept as it is inexpensive and readily

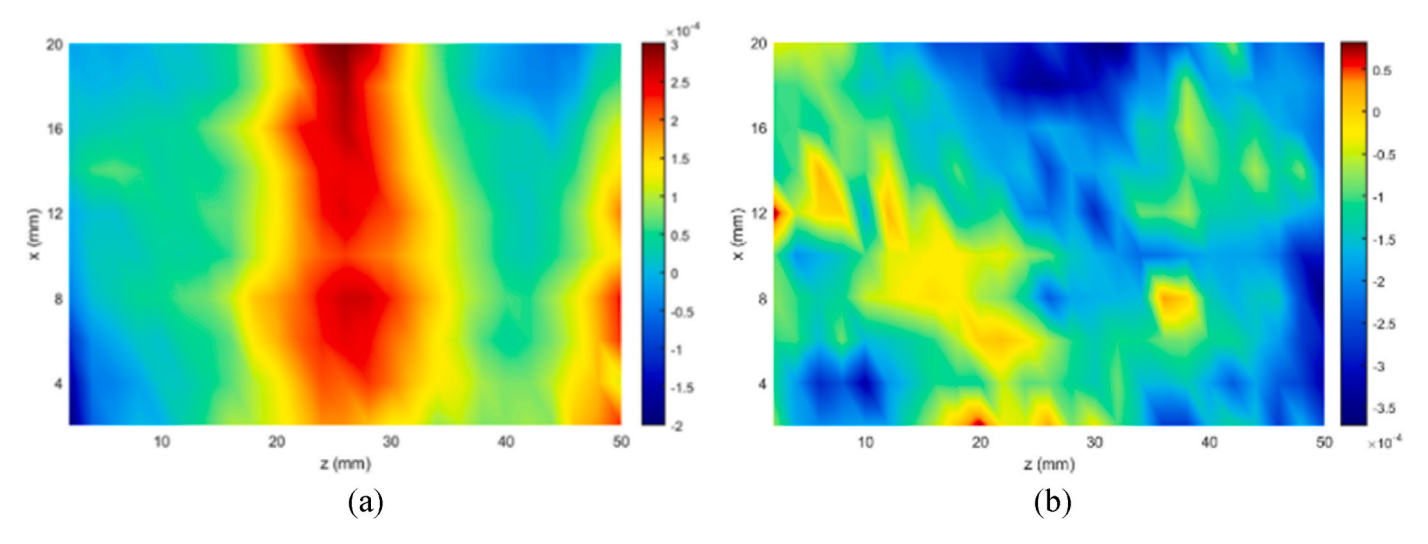


Fig. 15. Imaging results (a) with lens (b) without lens.

available substrate material. Using lower loss substrate materials will significantly improve the resolution of the system and will be undertaken as future work. On the other hand, the sensor to object stand-off distance can be increased further by increasing the thickness of the lens. However, increasing the thickness will increase the losses and hence the resolution will degrade. The stand-off distance for this study was limited to 1.67λ . It is predicted that by designing thicker lenses with low loss unit cells, the stand-off distance for subwavelength imaging can be further increased to multiple wavelengths. Additional plans are underway to investigate this aspect as part of future work.

Contributions

Srijan Datta: Data curation, Formal analysis, Investigation, Methodology, Validation, Original draft.

Lalita Udpa: Funding acquisition, Project administration, Resources, Supervision, Review & Editing.

Funding

This work was supported in part by the National Science Foundation Manufacturing USA Award #1762331 and in part by the American Society for Nondestructive Testing Fellowship Award 2021.

Declaration of competing interest

The authors declare the following financial interests/personal relationships which may be considered as potential competing interests: Lalita Udpa reports financial support was provided by National Science Foundation. Lalita Udpa reports financial support was provided by American Society for Nondestructive Testing.

Data availability

Data will be made available on request.

Appendix

Synchronous homodyne detection has been one of the most frequently used signal processing techniques for decades. It is a simple demodulation technique that suppresses excessive noise components and provide stable access to information that is encoded into the phase of the received signal. High signal to noise ratio associated with coherent homodyne detection allows lossy engineered NIM lens to be implemented in free space under practical conditions without the use of amplifiers or microwave absorbers.

The operating principle of a homodyne detection system can be understood from the following equations. The sinusoidal output V_{LO} of the RF signal generator, which is used to excite the experiment setup and feed the LO port of the mixer is of the form

$$V_{LO} = V_{ref} \left(\sin \omega_{ref} t + \theta_{ref} \right) \tag{A1}$$

where, V_{ref} , ω_{ref} and θ_{ref} are the amplitude, frequency, and phase of the RF signal generator output respectively. The received signal V_{RF} at the RF port of the mixer will be a sinusoid of the same frequency but different amplitude and phase given by

$$V_{RF} = V_{rec} (\sin \omega_{rec} t + \theta_{rec})$$
 (A2)

where, V_{rec} , and θ_{rec} are the amplitude, and phase of the received signal at the RF port respectively. The output V_{IF} at the IF port of the mixer is the product of the two sine waves given by,

$$V_{IF} = V_{LO}V_{RF} V_{IF} = V_{ref} \left(\sin \omega_{ref} t + \theta_{ref} \right) V_{rec} \left(\sin \omega_{ref} t + \theta_{rec} \right) V_{IF} = \frac{1}{2} V_{ref} V_{rec} \cos \left(\left[\omega_{ref} - \omega_{ref} \right] t + \theta_{rec} - \theta_{ref} \right) - \frac{1}{2} V_{ref} V_{rec} \cos \left(\left[\omega_{ref} + \omega_{ref} \right] t + \theta_{rec} + \theta_{ref} \right) \right)$$
(A3)

It can be seen from equation (A3) that the first term is a DC signal of the form

$$V_{DC} = \frac{1}{2} V_{ref} V_{rec} \cos(\theta_{rec} - \theta_{ref}) \tag{A4}$$

 V_{DC} produced at the IF port of the mixer is read in by the digital multimeter which encodes the phase information of the received signal (image

field) intensity.

References

- Abou-Khousa MA, Rahman MSU, Xingyu X. Dual-polarized microwave imaging probe. IEEE Sensor J 2019;19(5):1767–76. https://doi.org/10.1109/ JSEN.2018.2882695. 1 March1.
- [2] Ahadi M, Isa M, Saripan MI, Hasan WZW. Three dimensions localization of tumors in confocal microwave imaging for breast cancer detection. Microw Opt Technol Lett 2015;57(12):2917–29. https://doi.org/10.1002/mop.29470.
- [3] Paul S, Akhtar MJ. Novel metasurface lens-based RF sensor structure for SAR microwave imaging of layered media. IEEE Sensor J 2021;21(16):17827–37. https://doi.org/10.1109/JSEN.2021.3084614. 15 Aug.15.
- [4] Chudpooti N, et al. In-situ self-aligned NaCl-solution fluidic-integrated microwave sensors for industrial and biomedical applications. IEEE Access 2020;8: 188897–907. https://doi.org/10.1109/ACCESS.2020.3031864.
- [5] Sheen DM, McMakin DL, Hall TE. Three-dimensional millimeter-wave imaging for concealed weapon detection. IEEE Trans Microw Theor Tech 2001;49(9):1581–92. https://doi.org/10.1109/22.942570.
- [6] Witten AJ, Molyneux JE, Nyquist JE. Ground penetrating radar tomography: algorithms and case studies. IEEE Trans Geosci Rem Sens 1994;32(2):461–7. https://doi.org/10.1109/36.295060.
- [7] Kharkovsky S, Zoughi R. Microwave and millimeter wave nondestructive testing and evaluation - overview and recent advances. IEEE Instrum Meas Mag April 2007;10(2):26–38. https://doi.org/10.1109/MIM.2007.364985.
- [8] Mukherjee S, Udpa L, Udpa S, Rothwell EJ. Target localization using microwave time-reversal mirror in reflection mode. IEEE Trans Antenn Propag Feb. 2017;65 (2):820–8. https://doi.org/10.1109/TAP.2016.2627011.
- [9] Markley L, Eleftheriades GV. Two-dimensional subwavelength-focused imaging using a near-field probe at a λ/4 working distance. J Appl Phys 2010;107(9). https://doi.org/10.1063/1.3407518.
- [10] Mukherjee S, Su Z, Udpa L, Udpa S, Tamburrino A. Enhancement of microwave imaging using a metamaterial lens. IEEE Sensor J 2019;19(13):4962–71. https://doi.org/10.1109/JSEN.2019.2903454. 1 Julv1.
- [11] Schuster Arthur. An introduction to the theory of optics. E. Arnold; 1904.
- [12] Veselago VG [in Russian]. The electrodynamics of substances with simultaneously negative values of ϵ and μ , 92. Usp. Fiz. Nauk; 1967. p. 517–26. ; English translation in Sov. Phys. Uspekhi, 10, 1968, pp. 509–514.
- [13] Mandel'shtam LI. Group velocity in crystalline arrays [in Russian] Zh Eksp Teor Fiz 1945;15:475–8. also in Polnoe Sobraniye Trudov, 2, Leningrad, Izdat. Akad. Nauk SSSR, 1947, pp. 334–338.
- [14] Sivukhin DV. The energy of electromagnetic fields in dispersive media [in Russian] Opt Spektrosk 1957;3:308–12.
- [15] Smith DR, Padilla WJ, Vier DC, Nemat-Nasser SC, Schultz S. Composite medium with simultaneously negative permeability and permittivity. Phys Rev Lett May 2000;84(18):4184–7. https://doi.org/10.1103/PhysRevLett.84.4184.
- [16] Pendry JB, Holden AJ, Robbins DJ, Stewart WJ. Magnetism from conductors and enhanced nonlinear phenomena. IEEE Trans Microw Theor Tech 1999;47(11). https://doi.org/10.1109/22.798002.
- [17] Pendry JB, Holden AJ, Stewart WJ, Youngs I. Extremely low frequency plasmons in metallic mesostructures. Phys Rev Lett 1996;76(25). https://doi.org/10.1103/ PhysRevLett.76.4773.
- [18] Shelby RA, Smith DR, Schultz S. Experimental verification of a negative index of refraction. Science 2001 Apr 6;292(5514):77–9. https://doi.org/10.1126/ science.1058847.
- [19] Cui, Jun Tie, Smith David R, Liu Ruopeng. Metamaterials. Boston, MA, USA: springer; 2010.
- [20] Alù A. First-principles homogenization theory for periodic metamaterials. Phys Rev B Condens Matter 2011;84(7). https://doi.org/10.1103/PhysRevB.84.075153.
- [21] Slovick BA, Yu ZG, Krishnamurthy S. Generalized effective-medium theory for metamaterials. Phys Rev B Condens Matter 2014;89(15). https://doi.org/10.1103/ PhysRevB.89.155118.
- [22] Pendry JB. Negative refraction makes a perfect lens. Phys Rev Lett 2000;85(18). https://doi.org/10.1103/PhysRevLett.85.3966.
- [23] Smith David R, Pendry John B, Ck Wiltshire Mike. Metamaterials and negative refractive index. Science 2004;305(5685):788–92.
- [24] Smith DR, Schurig D, Rosenbluth M, Schultz S, Ramakrishna SA, Pendry JB. Limitations on subdiffraction imaging with a negative refractive index slab. Appl Phys Lett 2003;82(10). https://doi.org/10.1063/1.1554779.
- [25] Grbic A, Eleftheriades GV. Overcoming the diffraction limit with a planar left-handed transmission-line lens. Phys Rev Lett 2004;92(11). https://doi.org/10.1103/PhysRevLett.92.117403.
- [26] Ozbay E, Li Z, Aydin K. Super-resolution imaging by one-dimensional, microwave left-handed metamaterials with an effective negative index. J Phys Condens Matter 2008;20(30). https://doi.org/10.1088/0953-8984/20/30/304216.
- [27] Roy T, Rogers ETF, Zheludev NI. Sub-wavelength focusing meta-lens. Opt Express 2013;21(6). https://doi.org/10.1364/oe.21.007577.
- [28] Zhang Xiang, Liu Zhaowei. Superlenses to overcome the diffraction limit. Nat Mater 2008;7(6):435–41.

- [29] Mukherjee S, Shi X, Udpa L, Udpa S, Deng Y, Chahal P. Design of a split-ring resonator sensor for near-field microwave imaging. IEEE Sensor J 2018;18(17): 7066–76. https://doi.org/10.1109/JSEN.2018.2852657. 1 Sept.1.
- [30] Tabib-Azar M, Chowdhury MAH. A 10 GHz metamaterial sensor to detect SARS COV-2 and dust particles in free space. IEEE Sensor J 2022;22(13):12846–51. https://doi.org/10.1109/JSEN.2022.3178049. 1 July1.
- [31] Chuma EL, Iano Y, Fontgalland G, Bravo Roger LL. Microwave sensor for liquid dielectric characterization based on metamaterial complementary split ring resonator. IEEE Sensor J 2018;18(24):9978–83. https://doi.org/10.1109/ JSFN.2018.2872859. 15 Dec.15.
- [32] Ali A, El Badawe M, Ramahi OM. Microwave imaging of subsurface flaws in coated metallic structures using complementary split-ring resonators. IEEE Sensor J Sept.15, 2016;16(18):6890–8. https://doi.org/10.1109/JSEN.2016.2587738.
- [33] Ebrahimi A, Withayachumnankul W, Al-Sarawi S, Abbott D. High-sensitivity metamaterial-inspired sensor for microfluidic dielectric characterization. IEEE Sensor J May 2014;14(5):1345–51. https://doi.org/10.1109/JSEN.2013.2295312.
- [34] Melik R, Unal E, Perkgoz NK, Puttlitz C, Demir HV. Metamaterial-based wireless RF-MEMS strain sensors. Sensors 2010:2173–6. https://doi.org/10.1109/ ICSENS.2010.5690582. 2010 IEEE.
- [35] Puentes M, Schüssler M, Penirschke A, Damm C, Jakoby R. Metamaterials in microwave sensing applications. Sensors 2010:2166–71. https://doi.org/10.1109/ ICSENS.2010.5690570. 2010 IEEE.
- [36] Savin Adriana, et al. Enhancement of spatial resolution using a metamaterial sensor in nondestructive evaluation. Appl Sci 2015;5(4):1412–30.
- [37] Shreiber D, Gupta M, Cravey R. Microwave nondestructive evaluation of dielectric materials with a metamaterial lens. Sensor Actuator Phys 2008;144(1):48–55. https://doi.org/10.1016/j.sna.2007.12.031. ISSN 0924-4247.
- [38] Datta S, Mukherjee S, Shi X, Haq M, Deng Y, Udpa L, Rothwell E. Negative index metamaterial lens for subwavelength microwave detection. Sensors 2021;21(14): 4782. https://doi.org/10.3390/s21144782.
- [39] Datta Srijan, et al. Subwavelength microwave imaging system using a negative index metamaterial lens. ASNT Research Symposium 2022. https://doi.org/ 10.32548/RS.2022.007.
- [40] Noll DC, Nishimura DG, Macovski A. Homodyne detection in magnetic resonance imaging. IEEE Trans Med Imag June 1991;10(2):154–63. https://doi.org/10.1109/ 42.70473
- [41] Abbas GL, Chan VWS, Yee TK. Local-oscillator excess-noise suppression for homodyne and heterodyne detection. Opt Lett 1983;8(8):419–21.
- [42] Raymer MG, et al. Ultrafast measurement of optical-field statistics by dc-balanced homodyne detection. JOSA B 1995;12(10):1801–12.
- [43] Wilson Jeffrey, Schwartz Zachary. Multifocal flat lens with left-handed metamaterial. Appl Phys Lett 2005;86. https://doi.org/10.1063/1.1850590. 021112.021112.
- [44] Smith David R, Norman Kroll. Negative refractive index in left-handed materials. Phys Rev Lett 2000;85(14):2933.
- [45] Lagarkov AN, Kissel VN. Near-perfect imaging in a focusing system based on a left-handed-material plate. Phys Rev Lett 2004 Feb 20;92(7):077401. https://doi.org/10.1103/PhysRevLett.92.077401. Epub 2004 Feb 18. PMID: 14995884.
- [46] Zhang Shu, Yin Leilei, Fang Nicholas. Focusing ultrasound with an acoustic metamaterial network. Phys Rev Lett 2009;102(19):194301.
- [47] Walker Ezekiel L, et al. Sub-wavelength lateral detection of tissue-approximating masses using an ultrasonic metamaterial lens. Nat Commun 2020;11(1):1–13.
- [48] Xiang L, Jian L, Xinjing H. Acoustic meta-lens for enhanced sensing consisting of single-helicoid array. IEEE Sensor J 2022;22(14):13989–98. https://doi.org/ 10.1109/JSEN.2022.3181981. 15 July15.
- [49] Ozbay Ekmel, Li Zhaofeng, Aydin Koray. Super-resolution imaging by onedimensional, microwave left-handed metamaterials with an effective negative index. J Phys Condens Matter 2008;20(30):304216.
- [50] Wang G, Fang J, Dong X. Resolution of near-field microwave target detection and imaging by using flat LHM lens. IEEE Trans Antenn Propag Dec. 2007;55(12): 3534–41. https://doi.org/10.1109/TAP.2007.910365.
- [51] Mukherjee Saptarshi, Tamburrino Antonello, Haq Mahmoodul, Udpa Satish, Udpa Lalita. Far field microwave NDE of composite structures using time reversal mirror. NDT E Int 2018;93:7–17. https://doi.org/10.1016/j.ndteint.2017.09.008. ISSN 0963-8695.
- [52] Bakhtiari S, Qaddoumi N, Ganchev SI, Zoughi R. Microwave noncontact examination of disbond and thickness variation in stratified composite media. IEEE Trans Microw Theor Tech March 1994;42(3):389–95. https://doi.org/10.1109/ 22.277431
- [53] Qaddoumi N, El-hag AH, Al Hosani M, Mansouri IA, Ghufli HA. Detecting defects in outdoor non-ceramic insulators using near-field microwave non-destructive testing. IEEE Trans Dielectr Electr Insul April 2010;17(2):402–7. https://doi.org/ 10.1109/TDFL2010.5448094.
- [54] Li J, Liu C. Noncontact detection of air voids under glass epoxy jackets using a microwave system. Subsurf Sens Technol Appl 2001;2:411–23. https://doi.org/ 10.1023/A:1013221118462.